Meccanica (2021) 56:2599–2612
https://doi.org/10.1007/s11012-021-01389-1

Theoretical analysis of the energy conversion and vibration control characteristics of a slanted beam termination

Yingyu Hua · Emiliano Rustighi · Li Cheng · Waion Wong

Received: 12 January 2021 / Accepted: 7 June 2021 / Published online: 1 July 2021

Abstract The fundamental beam structure is often regarded as a wave or energy carrier in a wide range of research topics for structural engineering. Nevertheless, in the related literature the beam is positioned either horizontally or vertically, which may limit its application flexibility. Very few studies have investigated the energy conversion and vibration control characteristics induced by the flexural and axial waves coupling at a slanted angle discontinuity. This research aims to investigate the dynamic characteristics of a slanted beam termination (SBT), a finite beam with one end attached to a host structure and the other end free in a slant configuration. A generic wave-based formulation is developed to obtain both the waveguides distribution and the point impedance of the SBT taking the flexural and axial waves coupling into account. The semi-infinite beam (SIB) with the proposed SBT case is compared with the classic two SIBs case in terms of the energy conversion phenomena influenced by the connection angle and frequency. In the SIB with the SBT case, a certain connection angle will enable the SBT to achieve a substantial energy conversion at its resonance. From the vibration control perspective, a benchmark cantilevered beam is adopted to examine the SBT's vibration control performance theoretically and is verified experimentally. This research lays the foundation for the design of the beam-like device for energy conversion and vibration suppression by the variation of connection angle rather than the conventional tuning method based on the stiffness, mass and damping.

Keywords Wave · Beam · Connection angle · Energy conversion · Vibration control

Y. Hua (✉) · L. Cheng · W. Wong
Department of Mechanical Engineering, The Hong Kong Polytechnic University, Hong Kong, China
e-mail: yingyu.hua@connect.polyu.hk

Y. Hua
Department of Civil and Environmental Engineering, The Hong Kong Polytechnic University, Hong Kong, China

E. Rustighi
Department of Industrial Engineering, University of Trento, Trento, Italy

1 Introduction

The fundamental beam structure has facilitated preliminary development in a wide range of structural vibration acoustics research areas such as power flow analysis [1–3] and statistical energy analysis (SEA) [4–6]. From the application perspective, reductions of the flexural wave's power or magnitude and the lateral movement within a beam structure have been playing the role of paradigms for the implementation and testing of various control strategies in the field of

structure vibration [7–16] and structure-borne noise attenuation [17–20].

Although the fundamental beam structure was employed in extensive studies for vibration/ wave/ energy analysis, it was always regarded either as a wave or energy carrier or a stiffness element, and very few studies [21–27] considered the beam structure as an independent vibration attenuation device taking both its inertial mass and stiffness into account. Nashif and Jones [21] and Jones et al. [22] proposed a light resonant beam damper with a relatively wide frequency bandwidth. Extra damping and stiffness were offered by the viscoelastic attachment to the host structure. Jacquot [23] established the distributed parametric model of the free-free beam absorber with its center connected to the plant so that the stiffness and mass were provided by the beam absorber alone. The same distributed parametric model was adopted by Snowdon et al. [24] to develop the orthogonal crossed double beam dynamic vibration absorber (DVA) tuned to control the vibration of a continuous clamped-clamped beam and a plate respectively. But the distributed parametric model contained only the first mode information of a free-free beam. More modes were involved by Arpaci and Savci [25] and Aida et al. [26] when the cantilevered beam was used as an absorber. Hua et al. [27] suggested an analogy between a vertical beam and a conventional DVA when it was attached to a host cantilevered beam for localized vibration suppression. These studies all provided helpful modeling approaches to embody the beam structure in the host system. However, in these configurations, the beam must be laid horizontally or vertically to the host structure. Meanwhile, the impedance and mobility concepts of beam and plate structures were introduced to facilitate the acoustic analysis in the past two decades (Fahy and Gardonio [6]; Gardonio and Brennan [28], Cremer and Heckl [20]). But inadequate attention was paid to apply the beam's impedance to the vibration attenuation researches. Intuitively, the question arises whether a finite beam attached to the host structure at a slanted connection angle could be analogous to a vibration attenuation device or offer other benefits.

The second issue arises from the knowledge that various factors are leading to the coupling of the transverse wave and axial waves in the one-dimensional (1D) structural components, e.g., the existence of joints or junctions (Cremer and Heckl [20]), the simply-supported beam with one end attached to the tilted rolling surface (Ginsberg [29]) in the practical environment. Although the reflection and transmission ratios generated by the joints/junctions with a connection angle within the 1D structure have been studied extensively (Renno and Mace [30]; Langley and Heron [31]; Horner and White [32]), the correlation between the wave coupling and the force transmission has not been fully comprehended.

Inspired by the above issues the current paper proposes a slanted finite beam whose local coordinate axis has a certain connection angle of β(degree) with the host structure's axis. It has one end attached to the host structure and the other end free, hence is termed as the slanted beam termination (SBT). To date, a standard framework to correlate the waveguide distribution and force transmission analysis for the SBT structure has yet to be generated. Whether it is analogous to a conventional DVA is also worth investigation.

This paper aims to gain some insights into the design and analysis of beam-like structures from both the energy conversion and vibration control perspectives. Following the introduction, a wave-based formulation describing a generic case where the bidirectional incident waves coexist before and after the angle discontinuity in the two semi-infinite beams is introduced in Sect. 2.1. Then the slanted semi-infinite beam is changed to the finite SBT structure to obtain the reflection matrix in the primary semi-infinite beam. The point impedance of the SBT structure is also derived under the host coordinate in Sect. 2.2. Based on the wave-based formulation, the semi-infinite beam (SIB) with the proposed SBT case is compared with the classic two SIBs case in terms of the energy conversion phenomena influenced by the connection angle and frequency in Sect. 3.1. In Sect. 3.2, the benchmark cantilevered beam model attached with the SBT is established based on the mobility and impedance method in Sect. 2.2 to investigate its potential benefits in vibration attenuation. Both theoretical analysis and experimental verification are presented. Relevant conclusions are presented in Sect. 4.

2 Wave formulation for the SBT at a connection angle discontinuity

2.1 Waveguide distribution of the SBT attached to a semi-infinite beam

The connection angle discontinuity existing the 1D beam system will generate the coupling between axial and flexural waves. For clarity, the case of two beams connected by a connection angle β is considered as shown in Fig. 1. To consider the coupling effect, at the connection point, four 1D waveguide vectors, namely, $\mathbf{q}_{\mathbf{A}}^{+}, \mathbf{q}_{\mathbf{A}}^{-}, \mathbf{q}_{\mathbf{B}}^{+}$ and $\mathbf{q}_{\mathbf{B}}^{-} \in \mathbb{C}^{3\times 1}$, each consisting of three components referring to the propagating and evanescent flexural wave magnitudes as well as the propagating axial wave magnitudes, are defined. The subscripts **A** and **B** refer to the horizontal and slanted beams, respectively. The symbols plus and minus refer to positive and negative directions in the two beams' local axes, respectively. The semi-infinite beam is termed as SIB for short. A detailed description of the waveguide vector formulation, as well as the derivation of the transmission and reflection matrices $\mathbf{T_{AB}}$, $\mathbf{T_{BA}}$, $\mathbf{R_{AB}}$ and $\mathbf{R_{BA}}$ mentioned below are given in Appendix 1.

The same system consisting of two SIBs is employed in Fig. 1a, b. The waveguide distribution in Fig. 1a is the same as Horner and White [32] where the incident waveguide $\mathbf{q}_{\mathbf{A}}^{+}$ is toward the discontinuity and the transmitted $\mathbf{q}_{\mathbf{B}}^{+}$ and reflected $\mathbf{q}_{\mathbf{A}}^{-}$ are generated. The reciprocal case where the incident $\mathbf{q}_{\mathbf{B}}^{-}$ goes toward the discontinuity is shown in Fig. 1b. Figure 1c demonstrates the SIB attached with the SBT. In Fig. 1c, the incident $\mathbf{q}_{\mathbf{A}}^{+}$ goes towards the discontinuity and generates the transmitted $\mathbf{q}_{\mathbf{B}}^{+}$ in the SBT. Due to the finite length of SBT, $\mathbf{q}_{\mathbf{B}}^{+}$ will be reflected at the free end and the reflected waveguide reaching the discontinuity is $\mathbf{q}_{\mathbf{B}}^{-}$.

This paper aims to establish a generalized wave formulation to describe the waveguide distribution. Therefore the transmission and reflection matrices are introduced. In Fig. 1a, the transmission matrix $\mathbf{T_{AB}} \in \mathbb{C}^{3\times 3}$ and the reflection matrix $\mathbf{R_{AB}} \in \mathbb{C}^{3\times 3}$ correlate the waveguides $\mathbf{q}_{\mathbf{A}}^{+}, \mathbf{q}_{\mathbf{A}}^{-}$ and $\mathbf{q}_{\mathbf{B}}^{+}$. In Fig. 1a, the wave transmission from horizontal to slanted beam is:

$$\begin{aligned} \mathbf{q}_{\mathbf{A}}^{-} &= \mathbf{R_{AB}}\mathbf{q}_{\mathbf{A}}^{+} \\ \mathbf{q}_{\mathbf{B}}^{+} &= \mathbf{T_{AB}}\mathbf{q}_{\mathbf{A}}^{+}. \end{aligned} \tag{1}$$

For the reciprocal case in Fig. 1b, the transmission matrix $\mathbf{T_{BA}} \in \mathbb{C}^{3\times 3}$ and the reflection matrix $\mathbf{R_{BA}} \in \mathbb{C}^{3\times 3}$ are defined to describe the wave transmission from slant to horizontal beam as follows:

$$\begin{aligned} \mathbf{q}_{\mathbf{A}}^{-} &= \mathbf{T_{BA}}\mathbf{q}_{\mathbf{B}}^{-} \\ \mathbf{q}_{\mathbf{B}}^{+} &= \mathbf{R_{BA}}\mathbf{q}_{\mathbf{B}}^{-}. \end{aligned} \tag{2}$$

Following Fig. 1a–c could be regarded as the superposition of their waveguide distributions. In

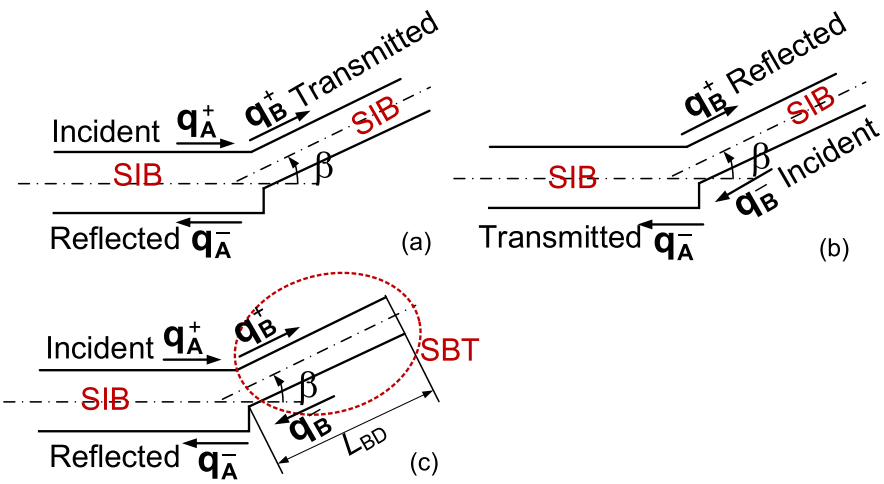

Fig. 1 The general waveguide distribution existing in the beam system with the discontinuity of β (degree) connection angle. **a** Two SIBs with $\mathbf{q}_{\mathbf{A}}^{+}$ as the incident waveguide; **b** two SIBs with $\mathbf{q}_{\mathbf{B}}^{-}$ as the incident waveguide; **c** one SIB and one SBT with $\mathbf{q}_{\mathbf{A}}^{+}$ as the incident waveguide ($\mathbf{q}_{\mathbf{A}}^{+}$ *and* $\mathbf{q}_{\mathbf{A}}^{-}$ are the horizontal beam's waveguide vectors for positive-going and negative-going waves. $\mathbf{q}_{\mathbf{B}}^{+}$ and $\mathbf{q}_{\mathbf{B}}^{-}$ are similarly defined for the slanted beam.)

Fig. 1c the bidirectional waveguides $\mathbf{q}_\mathbf{A}^+$ and $\mathbf{q}_\mathbf{B}^-$ coexist before and after the connection, the relationship between the four waveguides satisfies:

$$\begin{aligned}\mathbf{q}_\mathbf{A}^- &= \mathbf{R}_\mathbf{AB}\mathbf{q}_\mathbf{A}^+ + \mathbf{T}_\mathbf{BA}\mathbf{q}_\mathbf{B}^- \\ \mathbf{q}_\mathbf{B}^+ &= \mathbf{T}_\mathbf{AB}\mathbf{q}_\mathbf{A}^+ + \mathbf{R}_\mathbf{BA}\mathbf{q}_\mathbf{B}^-.\end{aligned} \tag{3}$$

Moreover, for the SBT structure, $\mathbf{q}_\mathbf{B}^-$ and $\mathbf{q}_\mathbf{B}^+$ could be correlated by the transfer matrix $\mathbf{T}_\mathbf{PR}$:

$$\mathbf{q}_\mathbf{B}^- = \mathbf{T}_\mathbf{PR}\mathbf{q}_\mathbf{B}^+, \tag{4}$$

where $\mathbf{T}_\mathbf{PR}$ equals the multiplication of the positive propagation matrix $\mathbf{P}_\mathbf{D}^+$, the reflection matrix $\mathbf{R}_\mathbf{F}$ at the free end and the negative propagation matrix $\mathbf{P}_\mathbf{D}^-$ in the SBT according to Mace (1984).

$$\mathbf{T}_\mathbf{PR} = \mathbf{P}_\mathbf{D}^-\mathbf{R}_\mathbf{F}\mathbf{P}_\mathbf{D}^+; \tag{5}$$

$$\mathbf{R}_\mathbf{F} = \begin{bmatrix} -i & 1+i & 0 \\ 1-i & i & 0 \\ 0 & 0 & 1 \end{bmatrix}, \quad \mathbf{P}_\mathbf{D}^+ = \begin{bmatrix} e^{-ik_bL_{BD}} & 0 & 0 \\ 0 & e^{-k_bL_{BD}} & 0 \\ 0 & 0 & e^{-ik_aL_{BD}} \end{bmatrix}$$

$$\mathbf{P}_\mathbf{D}^- = \begin{bmatrix} e^{ik_bL_{BD}} & 0 & 0 \\ 0 & e^{k_bL_{BD}} & 0 \\ 0 & 0\cdot & e^{ik_aL_{BD}} \end{bmatrix}.$$

where L_{BD}, k_b and k_a are for the finite length, the flexural and axial wavenumbers of the SBT.

Substituting Eqs. (5)–(3) yields the relationship between the positive waveguide $\mathbf{q}_\mathbf{A}^+$ and negative waveguide $\mathbf{q}_\mathbf{A}^-$ in the horizontal beam of Fig. 1c:

$$\mathbf{q}_\mathbf{A}^- = \left[\mathbf{R}_\mathbf{AB} + \mathbf{T}_\mathbf{BA}\mathbf{T}_\mathbf{PR}(\mathbf{I} - \mathbf{R}_\mathbf{BA}\mathbf{T}_\mathbf{PR})^{-1}\mathbf{T}_\mathbf{AB}\right]\mathbf{q}_\mathbf{A}^+ \tag{6}$$

Note that Eq. (6) should include but not be limited to the specific SBT structure in the present work. Any discontinuity or boundary conditions that generate the bidirectional waveguides $\mathbf{q}_\mathbf{A}^+$ and $\mathbf{q}_\mathbf{B}^+$ towards the discontinuity could be presented by Eq. (6) if the propagation matrix $\mathbf{T}_\mathbf{PR}$ is derived experimentally or numerically.

2.2 Point impedance of an SBT under host coordinate

The mechanical impedance and mobility approach arose from the electrical field at the end of the 19 century. Later, the electromechanical analogies were extended to both acoustic and mechanical researches. A comprehensive review was presented by Gardonion and Brennan [33]. Although the impedance and mobility concept for the flexible distributed structures, e.g., the 1D beam, rod, plate (Fahy and Gardonio [6]; Gardonio and Brennan [28], Cremer et al. [20]), have been formally presented, the impedance for the SBT has not been fully understood not to mention its application to vibration control.

The impedance matrices for a finite 1D beam $\mathbf{Z}_\mathbf{beam}$ and rod $\mathbf{Z}_\mathbf{rod}$ represents the transmission matrices between force $\mathbf{f}, \mathbf{f}_\mathbf{x}$ and velocity vectors $\mathbf{v}, \mathbf{v}_\mathbf{x}$ at the two ends in the beam and rod respectively as shown in Appendix 2. It is necessary to modify and assemble $\mathbf{Z}_\mathbf{beam}$ and $\mathbf{Z}_\mathbf{rod}$ to derive the point impedance of SBT with the free end and the coupling effects into consideration.

To clarify the problem, in Fig. 2 the local coordinate (x_2, y_2) of the SBT and the host coordinate (x_1, y_1) for the plant sharing the same origin at the connection point is defined. The host coordinate (x_1, y_1) is β degree clockwise with coordinate (x_2, y_2). In the local coordinate (x_2, y_2), the point impedance $\mathbf{Z}_\mathbf{c} \in \mathbb{C}^{3\times3}$ correlates the point force vector $\mathbf{f}_\mathbf{c}$ comprising the shear force S_1, moment M_1 and axial force F_{x1} and the point velocity vector $\mathbf{v}_\mathbf{c}$ comprising the lateral velocity $\dot{W}_1$, rotational velocity $\dot{\theta}_1$ and axial velocities $\dot{U}_1$ at the connection point

$$\begin{aligned}\mathbf{f}_\mathbf{c} &= \mathbf{Z}_\mathbf{c}\mathbf{v}_\mathbf{c}. \\ \mathbf{f}_\mathbf{c} &= \{S_1 M_1 F_{x1}\}^\mathrm{T} \\ \mathbf{v}_\mathbf{c} &= \left\{\dot{W}_1 \dot{\theta}_1 \dot{U}_1\right\}^\mathrm{T}.\end{aligned} \tag{7}$$

where $\mathbf{Z}_\mathbf{c}$ is the modified point impedance at coordinate (x_2, y_2):

$$\mathbf{Z}_\mathbf{c} = \begin{bmatrix} \mathbf{Z}_\mathbf{B} & 0 \\ 0 & \mathbf{Z}_\mathbf{R} \end{bmatrix}; \tag{8}$$

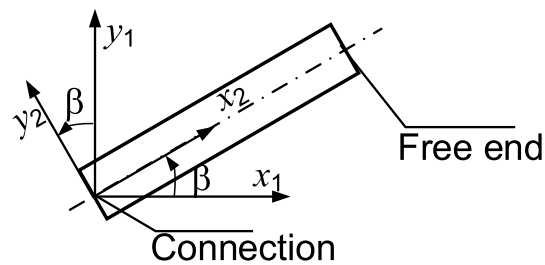

Fig. 2 The coordinates of the SBT (x_2, y_2) and the host system (x_1, y_1) with a connection angle of β (degree)

$$\mathbf{Z_B} = \mathbf{Z_{beam}}(1:2,1:2) - \mathbf{Z_{beam}}(1:2,3:4)$$
$$\mathbf{Z_{beam}^{-1}}(3:4,3:4)\mathbf{Z_{beam}}(3:4,1:2);$$
$$\mathbf{Z_R} = \mathbf{Z_{rod}}(1,1) - \mathbf{Z_{rod}}(1,2)\mathbf{Z_{rod}^{-1}}(2,2)\mathbf{Z_{rod}}(2,1).$$

where $\mathbf{Z_{beam}}(i:j,\ k:m)$ stands for the block matrix from the i^{th} row to the j^{th} row in the columns from k^{th} to m^{th} and $\mathbf{Z_{rod}}(i,m)$ for the element in the i^{th} row and the m^{th} column in the matrix.

To compute the effective forces and impedance transmitted to the plant, the force and velocity vectors and the impedance in the SBT coordinate $(x_2,\ y_2)$ should be transformed to the plant coordinate $(x_1,\ y_1)$ by the rotational matrix $\mathbf{R}$. To distinguish from the two coordinates, the variables with a tilde refer to the plant coordinate $(x_1,\ y_1)$. The force vector $\tilde{\mathbf{f}}_\mathbf{c} = \left\{\widetilde{S}_1\ \widetilde{M}_1\widetilde{F}_{x1}\right\}^{\mathrm{T}}$, the velocity vector $\tilde{\mathbf{v}}_\mathbf{c} = \left\{\dot{\widetilde{W}}_1\dot{\widetilde{\theta}}_1\ \dot{\widetilde{U}}\right\}^{\mathrm{T}}$, the impedance matrix $\tilde{\mathbf{Z}}_\mathbf{c}$ in the plant coordinate $(x1,\ y1)$ are related to $\mathbf{f_c}$ and $\mathbf{v_c}$ as:

$$\mathbf{f_c} = \mathbf{R}\tilde{\mathbf{f}}_\mathbf{c}, \tag{9a}$$

$$\mathbf{v_c} = \mathbf{R}\tilde{\mathbf{v}}_\mathbf{c} \tag{9b}$$

$$\tilde{\mathbf{f}}_\mathbf{c} = \tilde{\mathbf{Z}}_\mathbf{c}\tilde{\mathbf{v}}_\mathbf{c} \tag{9c}$$

where $\mathbf{R} = \begin{bmatrix} \cos\beta & 0 & -\sin\beta \\ 0 & 1 & 0 \\ \sin\beta & 0 & \cos\beta \end{bmatrix}$.

The point impedance $\tilde{\mathbf{Z}}_\mathbf{c}$ in the plant coordinate $(x_1,\ y_1)$ could thus be explicitly presented as

$$\tilde{\mathbf{Z}}_c = \mathbf{R}^T\mathbf{Z_c}\mathbf{R} = \begin{bmatrix} (\cos\beta)^2\mathbf{Z}_c(1,1) + (\sin\beta)^2\mathbf{Z}_c(3,3) & (\cos\beta)\mathbf{Z}_c(1,1) & (\sin\beta)(\cos\beta)[\mathbf{Z}_c(3,3) - \mathbf{Z}_c(1,1)] \\ (\cos\beta)\mathbf{Z}_c(1,2) & \mathbf{Z}_c(2,2) & -(\sin\beta)\mathbf{Z}_c(1,2) \\ (\sin\beta)(\cos\beta)[\mathbf{Z}_c(3,3) - \mathbf{Z}_c(1,1)] & -(\sin\beta)\mathbf{Z}_c(1,2) & (\cos\beta)^2\mathbf{Z}_c(3,3) + (\sin\beta)^2\mathbf{Z}_c(1,1) \end{bmatrix} \tag{10}$$

The emergence of the nonzero cross terms (i.e., $\tilde{\mathbf{Z}}_c(1,3)$, $\tilde{\mathbf{Z}}_c(2,3)$, $\tilde{\mathbf{Z}}_c(3,2)$ and $\tilde{\mathbf{Z}}_c(3,1)$) implies the coupling between the flexural and axial motions since the initial cross-terms in $\mathbf{Z_c}$ are zero. These cross-terms are at the core of the SBT's vibration control performance as to be discussed in Sect. 3.2.

3 Numerical example

3.1 The energy conversion characteristics of the SBT attached to the SIB

In this section, the specified case of the incident flexural wave from the horizontal beam is adopted to compare the energy conversion performance between the case of two SIBs in Fig. 1a and the case of one SIB with an SBT in Fig. 1c. Figure 3 presents the energy ratios of reflected and transmitted waves in the two SIBs of Fig. 1a under three different frequencies of 1 Hz/200 Hz/1000 Hz respectively. Under each frequency, the reflected flexural wave ratio η_{ff}, the reflected axial wave ratio η_{af}, the transmitted flexural wave ratio δ_{ff}, and the transmitted axial wave ratio δ_{af} are plotted against the connection angle. The reflected energy flexural and axial energy ratios in the SIB with an SBT structure in Fig. 1c are presented in Fig. 4a, b respectively.

The two beams have material properties and cross-sectional areas corresponding to a type of Aluminum alloy as shown in Table 1 whose parameters have been verified by the experiment in Sect. 3.2.2. All the parameter values in Table 1 are used throughout the paper. The SBT has a length of 90 mm with the cantilevered boundary condition such that its first flexural resonance appears at 180 Hz. The higher-order flexural and axial resonances are out of the frequency range of interest below 1000 Hz. No damping is considered in the following analysis to clarify the energy ratio's distribution among different waves.

Several phenomena are observed in Figs. 3 and 4. Notice that since no damping is added, the energy conservation law applies to both cases. In the two SIBs case in Fig. 3, the energy ratio summation of the four types of waves is unitary for any β at all frequencies. In the case of SIB with an SBT, the SBT will not dissipate

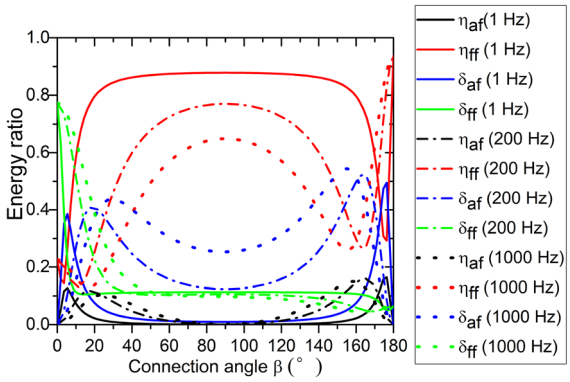

Fig. 3 The energy ratios of the transmitted and reflected waves in the two SIBs case in (Fig. 1a) at various frequencies with the incident flexural wave. Solid line (1 Hz); dash-dotted line (200 Hz); dotted line (1000 Hz) (η_{ff} reflected flexural wave energy ratio; η_{af} reflected axial wave energy ratio; δ_{ff} transmitted flexural wave energy ratio; δ_{af} transmitted axial wave energy ratio)

or transmit energy. Hence the incident flexural wave is only transmitted to the reflected flexural and axial waves in the SIB part. The summation of the flexural and axial wave energy is therefore unitary for any β at all frequencies as shown in Fig. 4. The energy ratios are extracted at the SBT's resonance of 180 Hz and off-resonance at 200Hz and shown in Fig. 5.

A second observation is the influence of frequency and β on the energy ratio distributions for both cases. For the two SIBs case in Fig. 3, the reflected flexural wave and transmitted axial wave dominates the energy distribution over a wide range of connection angle from 30° to 140°. The increase of β prohibits the transmission of the flexural wave. At certain β close to the horizontal configuration, the conversion between the flexural and axial waves becomes strongest. For instance, under 1 Hz case, the major conversion occurs at around 7° and 175° where the transmitted axial energy reaches a maximum of 50% overall connection angles. The variation of frequency will change the magnitude of energy ratios and the connection angle where the maximum conversion occurs. But the general energy distribution against β will not be substantially affected by the frequency change. This is attributed to the fact that no resonance exists in the two SIBs.

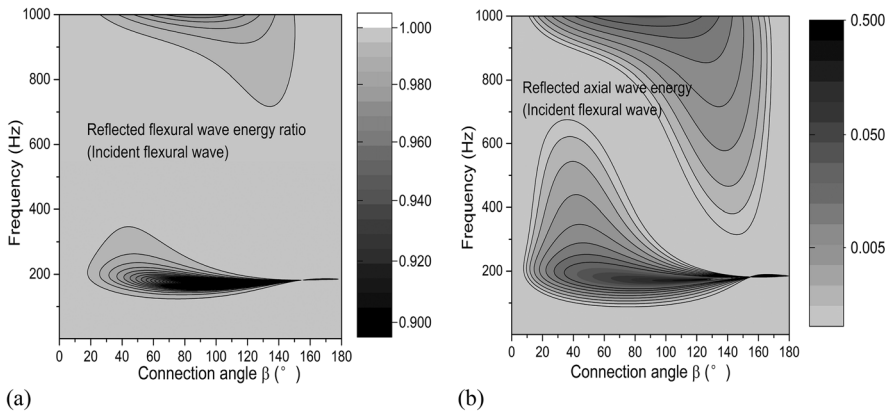

Fig. 4 The contour plot of the reflected energy ratios from SIB to SBT in (Fig. 1c) over the connection angle from 0° to 180° within the frequency range below 1000 Hz: **a** reflected flexural energy ratio (incident flexural wave); **b** reflected axial energy ratio (incident flexural wave)

Table 1 The parameters of the host beam and the SBT

	E (Pa)	ρ (Kg m^{-3})	Thickness (mm)	Width (mm)	Length* (mm)	First three natural* frequency
Host beam	55E^9	2700	6	20	360	34 Hz; 212 Hz; 592 Hz
SBT			2		90	180 Hz; 1130 Hz; 3160 Hz

*For the SIB structure, the length is infinite. But the young's modulus, the density, the thickness and the width still apply to the SIB structure

*The natural frequency is computed for the Host beam and SBT in Sect. 3.2.2

On the other hand, the energy ratios of the SIB with an SBT case show a relatively simple trend in Figs. 4 and 5. In the off-resonance frequencies, the reflected flexural wave dominates 90% of the total energy distribution at any β by comparing the flexural and axial ratios in Fig. 4. But at the resonance of 180 Hz, significant energy conversion occurs at about 150° making the reflected axial energy ratio jump from 10% to 65% as shown in Fig. 5.

Briefly, the energy distribution of the two SIBs case is more related to β variation than the frequency variation. The maximum energy conversion occurs for all frequencies at certain β close to the horizontal configuration.

But for the SIB with an SBT, the energy distribution is only sensitive to β variation at resonance but relative stable off-resonance. The maximum energy conversion could be achieved under a certain β at resonance.

3.2 Benchmark study of a host cantilevered beam connected with an SBT

3.2.1 The mobility and impedance model

This section aims to examine SBT's vibration control performance when it is attached to the free end of a benchmark cantilevered beam as shown in Fig. 6a. The assumptions of Sect. 2.2 for the force, velocity vectors and coordinates are used here. The control target is the response at the connection point $x_c = L_1$. An external force vector consisting of the lateral force at $x_e = L_1/2$ in terms of the unit white noise signal is written as $\mathbf{f_e} = \{100\}^T$ in the frequency domain. Replacing the SBT part with its control force vector $\tilde{\mathbf{f}}_\mathbf{c}$ exerted on $x_c = L_1$ yields Fig. 6b, showing that the motion of the primary beam is the summation of the contributions from the external force $\mathbf{f_e}$ and control force $\tilde{\mathbf{f}}_\mathbf{c}$. Based on the mobility and impedance formulation of beams (Gardonio and Brennan [28]), the velocity vector $\tilde{\mathbf{v}}_\mathbf{c}$ at the controlled point $x_c = L_1$ can be given as

$$\tilde{\mathbf{v}}_\mathbf{c} = \mathbf{Y_{ce}}\mathbf{f_e} + \mathbf{Y_{cc}}\tilde{\mathbf{f}}_\mathbf{c}. \tag{11}$$

where $\mathbf{Y_{ce}} \in \mathbb{C}^{3\times3}$ denotes the mobility from x_e to x_c and $\mathbf{Y_{cc}} \in \mathbb{C}^{3\times3}$ is the direct point mobility at x_c. These mobility matrices are assembled by the flexural and axial terms by the modal superposition method (Gardonio and Brennan [28]) in the fixed-free condition for both beams and rod as shown in Appendix 3. A total of 250 modal shape functions are used for the mobility matrices $\mathbf{Y_{cc}}$ and $\mathbf{Y_{ce}}$ to ensure the convergence of the results.

Substituting the point impedance matrix in Eqs. (10)–(11) yields the relationship between the velocity vector $\tilde{\mathbf{v}}_\mathbf{c}$, the acceleration vector $\tilde{\boldsymbol{a}}_\mathbf{c}$ and external force vector $\mathbf{f_e}$ with the SBT attached:

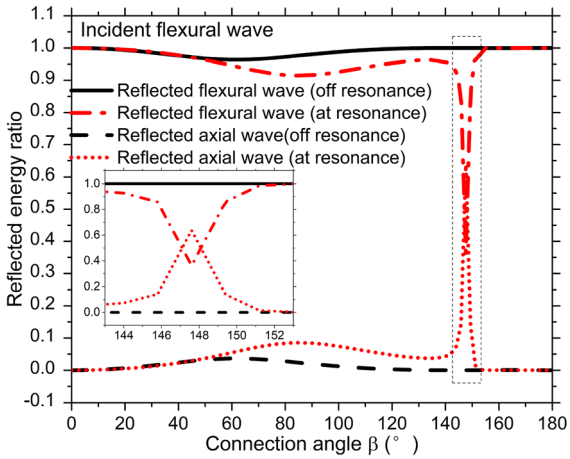

Fig. 5 The reflected energy ratios from SIB to SBT in (Fig. 1c) versus the connection angle β at the resonance of 180 Hz and off-resonance of 200Hz with the incident flexural wave; red dash-dotted line: reflected flexural energy at resonance; red dotted line: reflected axial energy at resonance; black solid line: reflected flexural energy off-resonance; black dashed line: reflected axial energy off-resonance

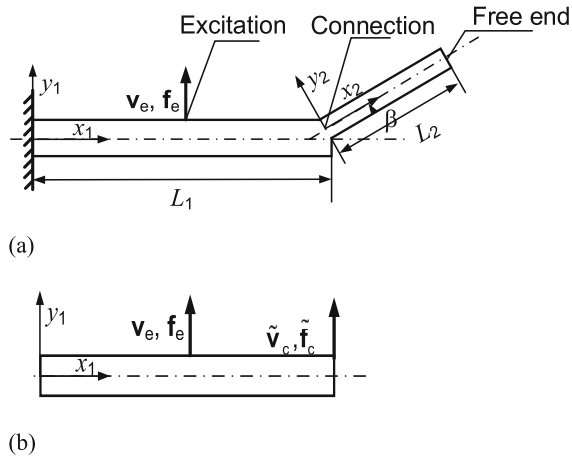

Fig. 6 The host cantilevered beam connected with an SBT at its free end **a** Coordinates (x_1, y_1) along the axis of host beam and Coordinates (x_2, y_2) along the axis of the SBT with the connection angle of β; **b** the velocity and force vectors at the excitation and connection points of the host cantilevered beam

$$\tilde{\mathbf{v}}_{\mathbf{c}} = \left[\mathbf{I} - \mathbf{Y}_{\mathbf{cc}}\tilde{\mathbf{Z}}_{\mathbf{c}}\right]^{-1}\mathbf{Y}_{\mathbf{ce}}\mathbf{f}_{\mathbf{e}}. \tag{12a}$$

$$\tilde{a}_{\mathrm{c}} = s\left[\mathbf{I} - \mathbf{Y}_{\mathbf{cc}}\tilde{\mathbf{Z}}_{\mathbf{c}}\right]^{-1}\mathbf{Y}_{\mathbf{ce}}\mathbf{f}_{\mathbf{e}}. \tag{12b}$$

where $s = i\omega$ denotes the Laplace transformation. The acceleration magnitude with unit excitation force is defined as accelerance. The analytical results of accelerance of the numerical model will be plotted in Fig. 8 8 to compare with the experiment measurement.

Recall that the reduction rate of the harmonically excited host single degree of freedom (SDOF) system response with control is given as (Brennan [34]):

$$X_{control}/X_{free} = 1/(1 + Z_{DVA}/Z_{primary}). \tag{13}$$

Assuming $\tilde{\mathbf{v}}_{\mathbf{c}\_free} = \mathbf{Y}_{\mathbf{ce}}\mathbf{f}_{\mathbf{e}}$ and $\mathrm{Z}_{\mathrm{primary}} = \mathbf{Y}_{\mathbf{cc}}^{-1}$, the expression for the ratio of the controlled response to the free vibration response is given as:

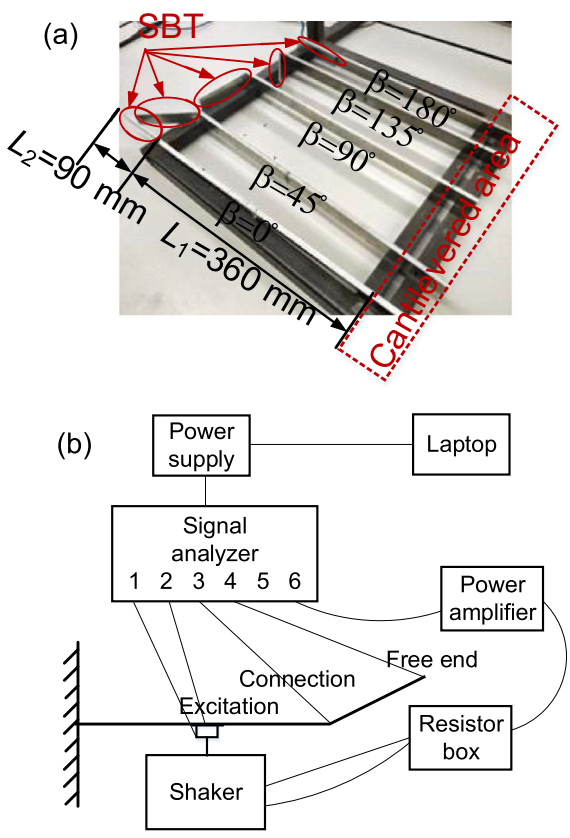

Fig. 7 Experimental preparation and setup **a** The five specimens bent to different connection angles (β = 0°/45°/90°/135°/180°; **b** Schematic of the experimental setup

$$\tilde{\mathbf{v}}_{\mathbf{c}} = \left[\mathbf{I} - \mathrm{Z}_{\mathrm{primary}}^{-1}\tilde{\mathbf{Z}}_{\mathbf{c}}\right]^{-1}\tilde{\mathbf{v}}_{\mathbf{c}\_free} \tag{14}$$

Note that the response ratio by SBT is similar to that by conventional DVA but in a matrix format. In this sense, the proposed SBT could be regarded as a specific type of DVAs.

3.2.2 *The experimental validation of the compound system dynamics*

To verify the previous theoretical model, an experimental test of the dynamics of the benchmark cantilevered beam attached to an SBT is conducted. Five specimens with the same properties for the host beam and SBT in Table 1 have been manufactured. As shown in Fig. 7a, the five specimens were bent to different connection angles representing β equaling $0°, 45°, 90°, 135°$ and $180°$ respectively. For the last two angles, welding was also necessary since a fracture at the connection point occurred, although extra damping was consequently introduced.

Figure 7b demonstrates a diagram of the experimental setup. A shaker excited the middle span of the host beam with a pseudorandom signal generated by the signal analyzer. A force gauge with a stinger measured the force signal exerted on the host beam, which was transferred to the analyzer as a reference signal. Three BK accelerometers were attached at the excitation point, the connection point and the free end of the SBT, respectively. The measured quantities were the complex accelerances, i.e., the ratio of acceleration to the force, at the three points. The sampling frequency is 2560 Hz. The interested frequency range is below 500 Hz so that only the first two modes of the host beam are presented. And the target is to suppress the second mode of the host beam.

Figure 8 compares the experimental accelerance magnitudes at the connection point under five different connection angles with the results from the previous theoretical impedance and mobility approach as from Eq. (11). The response at the free end of the host beam without SBT is also presented as a reference. According to Table 1, the first two resonances of the host beam are 34 Hz and 212 Hz respectively. The first resonance of SBT is 180 Hz close to the second resonance of the host beam. Consequently, the second mode at 212 Hz is split into two peaks or shifted due to the addition of SBT. In the cases of $\beta = 0°/45°$, the

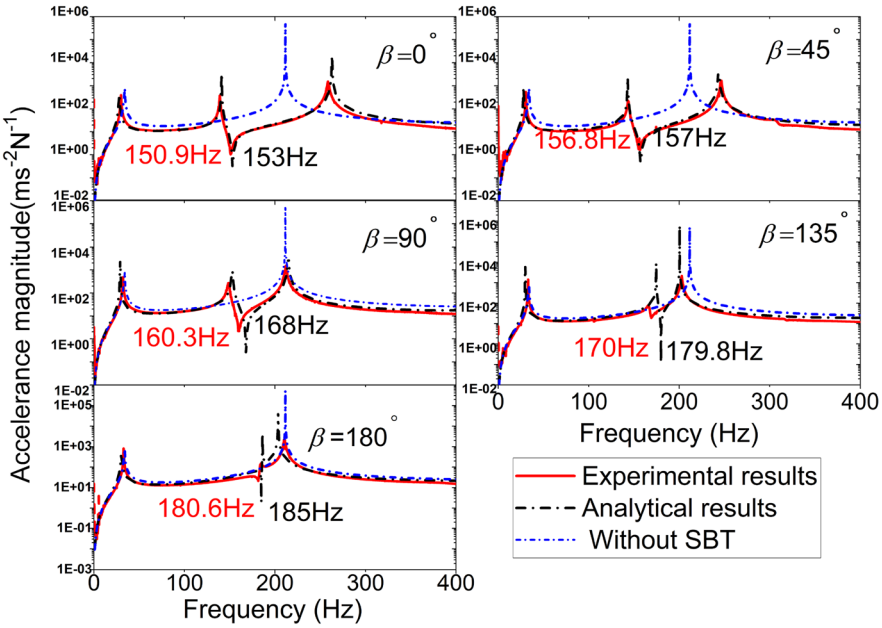

Fig. 8 The comparison between the experimental and theoretical accelerance magnitudes at the connection point (*y*-axis: Accelerance magnitude at the connection point (m s^{-2} N^{-1}); *x*-axis: Frequency (Hz) in the range from 0 to 400 Hz). Solid red line: experimental results; black dash-dotted line: theoretical results from Eq. (11); blue short-dashed line: the response at the free end of the host beam without SBT under the same excitation; number in red: the antiresonance of the experimental results; number in black: the antiresonance of the theoretical results

SBT is more like a conventional DVA that splits the host second mode into two peaks. But in the cases of $\beta = 90°/135°/180°$, the SBT will both add weight to the host beam and play its role as a DVA. Consequently, the second resonance will be shifted to the lower frequency range and be split into two.

In Fig. 8, the good agreement between experimental measurement and the theoretical results is also presented. In the 0° and 45° cases, there are only minor differences in the resonance and antiresonances, which might be due to the material damping mismatch since the theoretical model assumes no damping. There are relatively larger differences in the cases of $\beta = 90°/135°/180°$. It is postulated that these differences might be caused by the large deformation in the connection point and the extra damping introduced by the welded joints. More research will be conducted in the future to validate this.

Besides the resonance suppression, the antiresonance range covers about 30Hz frequency bandwidth when the connection angle increase from 0° to 180° according to both the experiment and theoretical results. This implies the application of SBT for forced vibration control when the system is subjected to varying frequency excitation. In combination with a certain physical control system(e.g., motor and micro control unit) it is possible to rotate the SBT in real-time to reach the appropriate angle that makes the controlled point reach antiresonance under that disturbance frequency. In this scenario, the SBT is like

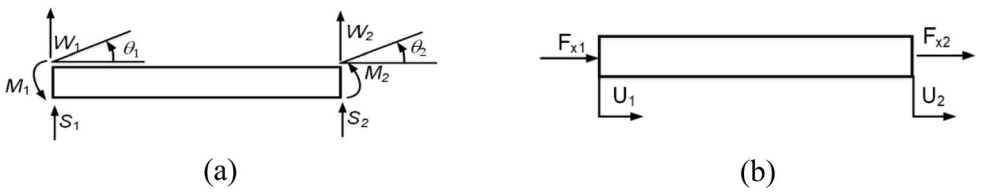

Fig. 9 **a** The shear forces, rotational moments, lateral displacement and rotational angle at the two ends of a finite uniform Euler–Bernoulli beam; **b** axial forces and displacements at the two ends of a finite uniform rod structure

the adaptive tuned vibration absorber (ATVA) with a variable stiffness or mass-distribution that can track the varying frequency excitation and make the host structure reach antiresonance at the disturbance frequency (Bonello and Beltrán-Carbajal [35]; Kidner and Brenna [36, 37]; Brennan [34]). A drawback of conventional ATVA is that although the vibration at the disturbance is suppressed, a new peak close to the disturbance frequency emerges leading to a narrow effective frequency range of ATVA (Brennan [34]). The host beam with the SBT shows that the antiresonance is quite separated from the two new peaks in the cases of $\beta = 0^\circ/45^\circ/90^\circ$, indicating appropriate frequency bandwidth.

Generally, the experimental results verify the accuracy of the model based on impedance and mobility theory. The results also imply that compared to conventional vibration absorber whose own dynamics is tuned for vibration control, it is also possible to implement the SBT into the host structure by changing the connection angle rather than its dynamics to reach the control target. In the future, more effort will be devoted to combining the SBT with the physical control system to achieve a large tunable range by changing the connection angle.

4 Conclusions

This study established a generic wave-based formulation for the dynamic analysis of a slanted beam termination (SBT) featured by the flexural and axial wave coupling. Moreover, this wave formulation can be extended to arbitrary boundary conditions and discontinuities, including but not limited to the slant angle and the free end. Based on the wave formulation, the energy conversion and vibration control characteristics of the SBT when it is attached to the host beam structure are identified and examined. The major conclusions are listed as follows.

(a) In terms of the reflected energy ratio, the SBT can convert incident wave energy very effectively when its axis is positioned to certain connection angles at resonance. Its energy conversion capability is less sensitive to the frequency and connection variation off-resonance. This phenomenon offers some guidance for the design of the termination.

(b) From the vibration control perspective, the point impedance of the SBT is also obtained through the wave formulation, implying their consistency. The benchmark cantilevered beam is adopted to build up the general mobility and impedance model when the SBT is attached to it. The experimental verification of the same structure agrees well with the response by the mobility and impedance method, indicating the accuracy of the model.

(c) In terms of resonance suppression, the SBT could act as the DVA at certain connections angles or simultaneously add weight to the plant and function as the DVA. In terms of adaptive vibration control under varying frequency excitation, the SBT could achieve a wide antiresonance frequency range by varying the connection angle. This implies that the connection angle could be regarded as a fourth tunable element for vibration control problems given that the conventional vibration control devices usually tune their own dynamics by changing the stiffness, mass and damping elements.

In the future, more effort will be devoted to expanding the wave formulation to more generic structures attached with an SBT. The current beam-based framework is suitable for the mechanical design as well as the vibration/acoustic control problems existing in the pipe system conveying fluid [38, 38], the flexible and long aerospace manipulator [40, 40], etc. A common issue existing in these structures is the vibration and the associated noise radiation affecting the service life and the environment. With some assumptions, these structures could be modeled by the Euler Bernoulli beam such that the theory in this paper could be applied. For instance, the pipe conveying fluid could be modeled by the beam with additional mass and damping terms related to the fluid speed and mass [38]. The proposed wave-based formulation of the slanted beam structure will benefit the wave, energy and vibration analysis of such structure in real practice and offer guidance for the arrangement and optimization of the beam-like system to minimize their vibration and elongate their service life.

Acknowledgements The authors appreciate the advice for improving the content and format during the writing process from Dr. Wenjing Sun and Dr. Haoran Zuo. The gratitude also

goes to the technical support from the technicians during the experiment.

Funding This study was not funded.

Declarations

Conflict of interest The authors declare that there is no conflict of interest.

Appendix A: Formulation of Reflection matrix and Transmission matrix

In Fig. 1a, suppose the incident waveguide $\mathbf{q}_\mathbf{A}^+$ is towards the connection point, a reflected waveguide $\mathbf{q}_\mathbf{A}^-$ in the horizontal beam and a transmitted waveguide $\mathbf{q}_\mathbf{B}^+$ are generated in the slanted beam respectively. Note that the two beams are semi-infinite, so $\mathbf{q}_\mathbf{B}^-$ does not exist in this case. The components in the waveguide vector comprise the wave magnitudes of both flexural and axial waves. In the horizontal section, the incident flexural wave W_{in} and axial wave U_{in} as well as the reflected flexural wave W_{rf} and axial wave U_{rf} coexist and they can be represented in the wave formulation.

$$W_{in} = A^+ e^{-ik_{b1}x_1} + A_N^+ e^{-k_{b1}x_1} \tag{15}$$

$$W_{rf} = A^- e^{ik_{b1}x_1} + A_N^- e^{k_{b1}x_1} \tag{16}$$

$$U_{in} = B^+ e^{-ik_{a1}x_1} \tag{17}$$

$$U_{rf} = B^- e^{ik_{a1}x_1} \tag{18}$$

where k_{b1} and k_{a1} are the wavenumbers for the flexural and axial waves in the horizontal beam, respectively. The incident waveguide and the reflected waveguide are therefore given as:

$$\mathbf{q}_\mathbf{A}^+ = \left[A^+ A_N^+ B^+\right]^T; \tag{19}$$

$$\mathbf{q}_\mathbf{A}^- = \left[A^- A_N^- B^-\right]^T. \tag{20}$$

In the slanted beam part, the transmitted flexural and axial waves W_{tm} and U_{tm} are given by:

$$W_{tm} = C^+ e^{-ik_{b2}x_1} + C_N^+ e^{-k_{b2}x_1}; \tag{21}$$

$$U_{tm} = D^+ e^{-ik_{a2}x_1}, \tag{22}$$

where k_{b2} and k_{a2} are the wavenumbers for the flexural and axial waves in the slanted beam, respectively.

The transmitted waveguide is then represented as:

$$\mathbf{q}_\mathbf{B}^+ = \left[C^+ C_N^+ D^+\right]. \tag{23}$$

The reflection and transmission matrices from A to B satisfy the following equilibrium:

$$\mathbf{q}_\mathbf{A}^- = \mathbf{R_{AB}}\mathbf{q}_\mathbf{A}^+; \tag{24}$$

$$\mathbf{q}_\mathbf{B}^+ = \mathbf{T_{AB}}\mathbf{q}_\mathbf{A}^+. \tag{25}$$

To derive the reflection and transmission matrices at the connection point in Fig. 1a, the force and displacement equilibriums are established.

$$\begin{cases} E_1 I_1 \dfrac{\partial^2 W_1}{\partial x_1^2} = E_2 I_2 \dfrac{\partial^2 W_2}{\partial x_2^2}; \\ E_1 S_1 \dfrac{\partial U_1}{\partial x_1} = E_2 S_2 \dfrac{\partial U_2}{\partial x_2}\cos\beta + E_2 I_2 \dfrac{\partial^3 W_2}{\partial x_2^3}\sin\beta; \\ E_1 S_1 \dfrac{\partial^3 W_1}{\partial x_1^3} = -E_2 S_2 \dfrac{\partial U_2}{\partial x_2}\sin\beta + E_2 I_2 \dfrac{\partial^3 W_2}{\partial x_2^3}\cos\beta; \\ U_1 = U_2\cos\beta - W_2\sin\beta \\ W_1 = U_2\sin\beta + W_2\cos\beta \\ \dfrac{\partial W_2}{\partial x_2} = \dfrac{\partial W_1}{\partial x_1}. \end{cases} \tag{26}$$

where $W_1 = W_{in} + W_{rf}$; $W_2 = W_{tm}$; $U_1 = U_{in} + U_{rf}$; $U_2 = U_{tm}$. Each column of $\mathbf{R_{AB}}$ and $\mathbf{T_{AB}}$ correspond to the transmission coefficient from the incident wave magnitude to the transmitted and reflected wave magnitude respectively. For instance, let $\mathbf{q}_\mathbf{A}^+ = [A^+\,0\,0]$, the first column of $\mathbf{R_{AB}}$ and $\mathbf{T_{AB}}$ could be derived by solving the above equations in Eq. (26). Similarly, when the incident wave is from the inverse direction, i.e., $\mathbf{q}_\mathbf{B}^-$ the incident wave, $\mathbf{q}_\mathbf{A}^-$ the transmitted wave and $\mathbf{q}_\mathbf{B}^+$ the reflected wave, the reflected and transmitted matrices $\mathbf{R_{BA}}$ and $\mathbf{T_{BA}}$ could be derived through the same process. The derivation of the transmission and reflection matrices when there is only a unidirectional incident waveguide is the same as presented in the study (Horner and White [32]). But when the bidirectional incident waveguides, i.e., $\mathbf{q}_\mathbf{B}^-$ and $\mathbf{q}_\mathbf{A}^+$ coexist, Eq. (1) in this paper should be employed to present the more general case.

After obtaining the waveguide magnitude through Eq. (26), the reflected and transmitted waves' energy

ratios to the incident wave could be derived. Take the incident propagating flexural wave as an example.

The energy ratio of the reflected flexural wave to the incident flexural wave is:

$$\eta_{ff} = \left(A^{-}/A^{+}\right)^{2} \tag{27}$$

The energy ratio of the reflected axial wave to the incident flexural wave is:

$$\eta_{af} = E_1 S_1 k_{a1} \left(B^{-}/A^{+}\right)^{2} / \left(2E_1 I_1 k_{b1}^{3}\right) \tag{28}$$

The energy ratio of the transmitted flexural wave to the incident flexural wave is

$$\delta_{ff} = \left(E_2 I_2 k_{b2}^{3} C^{+}\right)^{2} / \left(E_1 I_1 k_{b1}^{3} A^{+}\right)^{2} \tag{29}$$

The energy ratio of the transmitted flexural wave to the incident flexural wave is

$$\delta_{af} = \left(E_2 S_2 k_{a2} D^{+}\right)^{2} / \left(2E_1 I_1 k_{b1}^{3} A^{+}\right)^{2} \tag{30}$$

Appendix B: Wave approach formulation

Suppose there is a finite beam of length L. The origin of the reference coordinate system is assumed to start at the left end. The internal forces and velocities of the beam can be represented by the shear forces $\mathrm{S_i}$, rotational moments $\mathrm{M_i}$, lateral velocity $\dot{\mathrm{W}}_\mathrm{i}$ and angular velocity $\dot{\theta}_\mathrm{i}$. The subscript i=1 denotes the left end (x=0), while i=2 denotes the right end (x = L). The force and velocity vectors, **f** and v, are composed of the shear forces and moments, and the flexural and rotational velocities at the two ends, i.e., $\mathrm{f} = \mathrm{S_1 M_1 S_2 M_2}^{\mathrm{T}}$ and $\mathrm{v} = \left\{ \dot{W}_1 \quad \dot{\theta}_1 \quad \dot{W}_2 \quad \dot{\theta}_2 \right\}^{\mathrm{T}}$ as shown in Fig. 9a.

The lateral displacement at any point x along a beam can be interpreted as the superposition of positive and negative waves (Fahy and Gardonio 2007):

$$W(x) = A_1 e^{-ik_b x} + A_{1N} e^{-k_b x} + A_2 e^{ik_b x} + A_{2N} e^{k_b x}; \tag{31}$$

where $k_b = (\rho S/EI)^{1/4} \omega^{1/2}$ is the wavenumber of the flexural wave and A_1, A_2,$A_{1\mathrm{N}}$, $A_{2\mathrm{N}}$ are the complex magnitudes of the propagating and evanescent waves in both directions. Assuming the wave component vector $\mathbf{q} = \{A_1\, A_{1\mathrm{N}}\, A_2\, A_{2\mathrm{N}}\}^{T}$, the internal force vector f and the velocity vector v satisfy the following relationship:

$$\mathbf{f} = \mathbf{T}_1 \mathbf{q}; \mathbf{v} = \mathbf{T}_2 \mathbf{q} \tag{32}$$

where transfer matrices $\mathbf{T}_1, \mathbf{T}_2 \in \mathbb{C}^{4\times4}$ and the detailed expressions for $\mathbf{T}_1$ and $\mathbf{T}_2$ can be derived by the relationship between general forces, velocities, and wave magnitudes based on the waveform in Eq. (31). Consequently, the impedance matrix $\mathbf{Z_{beam}} \in \mathbb{C}^{4\times4}$ can be derived by $\mathbf{Z_{beam}} = \mathbf{T}_1 {\mathbf{T}_2}^{-1}$ as follows:

$$\mathbf{f} = \mathbf{Z_{beam}} \mathbf{v} = \frac{EIk_b^3}{j\omega N} \begin{bmatrix} -K_{11} & -P & K_{12} & V \\ -P & Q_{11} & -V & Q_{12} \\ K_{12} & -V & -K_{11} & P \\ V & Q_{12} & P & Q_{11} \end{bmatrix} \mathbf{v}; \tag{33}$$

where

$$\begin{aligned} K_{11} &= \cos(k_b L)\sinh(k_b L) + \sin(k_b L)\cosh(k_b L), \\ K_{12} &= \sinh(k_b L) + \sin(k_b L), \\ P &= \sinh(k_b L)\sin(k_b L)/k_b, \\ V &= [\cos(k_b L) - \cosh(k_b L)]/k_b \\ Q_{11} &= [\cos(k_b L)\sinh(k_b L) - \sin(k_b L)\cosh(k_b L)]/k_b^2 \\ Q_{12} &= [\sin(k_b L) - \sinh(k_b L)]/k_b^2, \\ N &= \cos(k_b L)\cosh(k_b L) - 1. \end{aligned} \tag{34}$$

Identically, the longitudinal direction's impedance $\mathbf{Z_{rod}} \in \mathbb{C}^{2\times2}$ can be derived by the wave formulation of a finite rod with length L in Fig. 9b. The axial waves existing in the rod are non-dispersive, so the axial displacement at any point x comprises only the propagating waves:

$$U(x) = B_1 e^{-ik_l x} + B_2 e^{ik_l x} \tag{35}$$

where $k_l = (\rho/E)^{1/2}\omega$ is the axial wavenumber and B_1 and B_2 are the complex magnitudes of the propagating waves in both directions. The force and velocity vectors $\mathbf{f_x} = \mathrm{F_{x1} F_{x2}}^{\mathrm{T}}$ and $\mathbf{v_x} = \dot{U}_1 \dot{U}_2^{\mathrm{T}}$ comprise the axial forces and velocities at the two ends.

$$\mathbf{f_x} = \mathbf{Z_{rod}} \mathbf{v_x} = \begin{bmatrix} Z_{11} & Z_{12} \\ Z_{21} & Z_{22} \end{bmatrix} \begin{Bmatrix} \dot{U}_1 \\ \dot{U}_2 \end{Bmatrix} \tag{36}$$

where

$$Z_{11} = -Z_{22} = -jS\sqrt{E\rho}\cot(k_l L), Z_{12} = -Z_{21} = jS\sqrt{E\rho}/\sin(k_l L).$$

The expressions for the impedance matrices are the same as those directly given by (Gardonio and Brennan [28]), where the procedure of obtaining these impedance matrices was not presented. This section validates the consistency between the wave approach and impedance matrix formulation.

Appendix C: Beam mobility formulation

The mobility formulation of the cantilevered host beam will be introduced with both axial and flexural motions being considered. The mobility matrix representing the transmission from the force vector at x_i to the velocity vector at x_j is given through the modal superposition (Gardonio and Brennan [28]) as:

$$\mathbf{Y_{ij}} = \begin{bmatrix} Y_{\dot{W}_j S_i} & Y_{\dot{W}_j M_i} & 0 \\ Y_{\dot{\theta}_j S_i} & Y_{\dot{\theta}_j M_i} & 0 \\ 0 & 0 & Y_{\dot{U}_j M_i} \end{bmatrix} \tag{37}$$

$$\begin{aligned} Y_{\dot{\theta}_j S_i} &= \sum_{n=1}^{\infty} \frac{i\omega \Psi_n'(x_j)\Psi_n(x_i)}{\rho SL\left[\omega_n^2(1+j\eta)-\omega^2\right]}, \\ Y_{\dot{\theta}_j M_i} &= \sum_{n=1}^{\infty} \frac{i\omega \Psi_n'(x_j)\Psi_n'(x_i)}{\rho SL\left[\omega_n^2(1+j\eta)-\omega^2\right]} \\ Y_{\dot{W}_j S_i} &= \sum_{n=1}^{\infty} \frac{i\omega \Psi_n(x_i)\Psi_n(x_j)}{\rho SL\left[\omega_n^2(1+j\eta)-\omega^2\right]}, \\ Y_{\dot{W}_j M_i} &= \sum_{n=1}^{\infty} \frac{i\omega \Psi_n'(x_i)\Psi_n(x_j)}{\rho SL\left[\omega_n^2(1+j\eta)-\omega^2\right]}, \\ Y_{\dot{U}_j F_{xi}} &= \sum_{m=1}^{\infty} \frac{i\omega \varphi_m(x_i)\varphi_m(x_j)}{\rho SL\left[\Omega_m^2(1+j\eta)-\omega^2\right]}, \end{aligned} \tag{38}$$

where $\Psi_n(x)$ and ω_n are the n^{th} modal shape function and the natural frequency of a cantilevered beam, respectively, and $\varphi_m(x)$ and Ω_m are the m^{th} modal shape function and the natural frequency of a fixed-free rod, respectively. The hysteresis damping ratio η is assumed to be material damping. It is set to zero in the main content.

References

1. Noiseux DU (1970) Measurement of power flow in uniform beams and plates. J Acoust Soc Am 47:238–247. https://doi.org/10.1121/1.1911472
2. Verheij JW (1980) Cross spectral density methods for measuring structure borne power flow on beams and pipes. J Sound Vib 70:133–138. https://doi.org/10.1016/0022-460X(80)90559-3
3. Pavic G (2007) Chapter 16 structure-borne energy flow. In: Handbook of noise vibration and control, pp 232–240. http://onlinelibrary.wiley.com/doi/abs/10.1002/9780470209707.ch16
4. Lyon RH, Eichler E (1964) Random vibration of connected structures. J Acoust Soc Am 36:1344–1354. https://doi.org/10.1121/1.1919207
5. Scharton TD, Lyon RH (1968) Power flow and energy sharing in random vibration. J Acoust Soc Am 43:1332–1343. https://doi.org/10.1121/1.1910990
6. Fahy F, Gardonio P (2007) Sound and stuctural vibration:radiation, transmission and response. Academic Press, London
7. Brennan MJ, Dayou J (2000) Global control of vibration using a tunable vibration neutralizer. J Sound Vib 232:585–600. https://doi.org/10.1006/jsvi.1999.2757
8. Dayou J, Brennan MJ (2002) Global control of structural vibration using multiple-tuned tunable vibration neutralizers. J Sound Vib 258:345–357. https://doi.org/10.1006/jsvi.5188
9. Dayou J, Brennan MJ (2003) Experimental verification of the optimal tuning of a tunable vibration neutralizer for global vibration control. Appl Acoust 64:311–323. https://doi.org/10.1016/S0003-682X(02)00067-1
10. Dayou J (2006) Fixed-points theory for global vibration control using vibration neutralizer. J Sound Vib 292:765–776. https://doi.org/10.1016/j.jsv.2005.08.032
11. Brennan MJJ (1998) Control of flexural waves on a beam using a tunable vibration neutraliser. J Sound Vib 222:389–407. https://doi.org/10.1006/jsvi.1998.2031
12. El-Khatib HM, Mace BR, Brennan MJ (2005) Suppression of bending waves in a beam using a tuned vibration absorber. J Sound Vib 288:1157–1175. https://doi.org/10.1016/j.jsv.2005.01.024
13. Issa JS (2019) Exact tuning of a vibration neutralizer for the reduction of flexural waves in beams. J Acoust Soc Am 146:486–500. https://doi.org/10.1121/1.5116690
14. Goyder HGD, White RG (1980) Vibrational power flow from machines into built-up structures, part I: introduction and approximate analyses of beam and plate-like foundations. J Sound Vib 68:59–75. https://doi.org/10.1016/0022-460X(80)90452-6
15. Pinnington RJ, White RG (1981) Power flow through machine isolators to resonant and non-resonant beams. J Sound Vib 75:179–197. https://doi.org/10.1016/0022-460X(81)90338-2
16. Koh YK, White RGG (1996) Analysis and control of vibrational power transmission to machinery supporting structures subjected to a multi-excitation system, part II: vibrational power analysis and control schemes. J Sound Vib 196:495–508. https://doi.org/10.1006/jsvi.1996.0497
17. Elliott SJ, Johnson ME (1993) Radiation modes and the active control of sound power. J Acoust Soc Am. https://doi.org/10.1121/1.407490
18. Gibbs GP, Fullerf CR (1992) Experiments on active control of vibrational power flow using piezoceramic actuators/

sensors. AIAA J. 30:457–463. https://doi.org/10.2514/3.10939
19. Fuller CR, Gibbs GP, Silcox RJ (1990) Simultaneous active control of flexural and extensional waves in beams. J Intell Mater Syst Struct 1:235–247
20. Cremer L, Heckl M, Petersson BA (2004) Structure-borne sound: structural vibrations and sound radiation at audio frequencies, 3rd edn. Springer, Berlin
21. Nashif AD, Jones DIG (1969) A resonant beam tuned damping device. J. Eng. Power 91:143–147
22. Jones DIG, Nashif AD, Stargardter H (1975) Vibrating beam dampers for reducing vibrations in gas turbine blades. J Eng Gas Turbines Power. https://doi.org/10.1115/1.3445888
23. Jacquot RG, Foster JE (1977) Optimal cantilever dynamic vibration absorbers. J Manuf Sci Eng 99:138–141
24. Snowdon JC, Wolfe AA, Kerlin RL (1984) The cruciform dynamic vibration absorber. J Acoust Soc Am 75:1792–1799. https://doi.org/10.1121/1.390980
25. Arpaci A, Savci M (1987) A cantilever beam damper suppressing rectangular plate vibrations. J Sound Vib 115:225–232
26. Aida T, Toda S, Ogawa N, Imada Y (1992) Vibration control of beams by beam-type vibration dynamic vibration absorbers. J Eng Mech 118:248–258
27. Hua Y, Wong W, Cheng L (2018) Optimal design of a beam-based dynamic vibration absorber using fixed-points theory. J Sound Vib 421:111–131. https://doi.org/10.1016/j.jsv.2018.01.058
28. Gardonio P, Brennan MJ (2018) Mobility and impedance methods in structural dynamics. Advanced applications in acoustics, noise and vibration. CRC Press, pp 403–461
29. Ginsberg JH (2009) Coupling of axial and transverse displacement fields in a straight beam due to boundary conditions. J Acoust Soc Am 126:1120–1124. https://doi.org/10.1121/1.3183368
30. Renno JM, Mace BR (2013) Calculation of reflection and transmission coefficients of joints using a hybrid finite element/wave and finite element approach. J Sound Vib 332:2149–2164. https://doi.org/10.1016/j.jsv.2012.04.029
31. Langley RS, Heron KH (1990) Elastic wave transmission through plate/beam junctions. J Sound Vib 143:241–253. https://doi.org/10.1016/0022-460X(90)90953-W
32. Horner JL, White RGG, Honer J, White RGG (1991) Prediction of vibration power transmission through bends and joints in beam-like structures. J Sound Vib 147:87–103
33. Gardonio P, Brennan MJ (2002) On the origins and development of mobility and impedance methods in structural dynamics. J Sound Vib. https://doi.org/10.1006/jsvi.2001.3879
34. Brennan MJ (1997) Vibration control using a tunable vibration neutralizer. Proc Inst Mech Eng C J Mech Eng Sci 211:91–107. https://doi.org/10.1243/0954406971521683
35. Bonello P (2011) Adaptive tuned vibration absorbers: design principles, concepts and physical implementation. Vib Anal Control New Trends Dev. https://doi.org/10.5772/23558
36. Kidner M, Brennan MJ (1999) Improving the performance of a vibration neutraliser by actively removing damping. J Sound Vib 221:587–606. https://doi.org/10.1006/jsvi.1998.2027
37. Kidner MRF, Brennan MJ (2001) Real-time control of both stiffness and damping in an active vibration neutralizer. Smart Mater Struct 10:758–769. https://doi.org/10.1088/0964-1726/10/4/321
38. Païdoussis MP, Li GX (1993) Pipes conveying fluid: a model dynamical problem. J Fluids Struct 7:137–204
39. Yu D, Wen J, Zhao H, Liu Y, Wen X (2011) Flexural vibration band gap in a periodic fluid-conveying pipe system based on the Timoshenko beam theory. J Vib Acoust Trans ASME 133:8–10. https://doi.org/10.1115/1.4001183
40. Yu XY, Chen L (2015) Singular perturbation adaptive control and vibration suppression of free-flying flexible space manipulators. Proc Inst Mech Eng C J Mech Eng Sci 229:1989–1997. https://doi.org/10.1177/0954406214551777
41. Sabatini M, Gasbarri P, Monti R, Palmerini GB (2012) Vibration control of a flexible space manipulator during on orbit operations. Acta Astronaut 73:109–121. https://doi.org/10.1016/j.actaastro.2011.11.012